Off-axis full-field swept-source optical coherence tomography using holographic refocusing

Dierck Hillmann[*,a], Gesa Franke[b,c], Laura Hinkel[b], Tim Bonin[b], Peter Koch[a], Gereon Hüttmann[b,c]

[a]Thorlabs GmbH, Maria-Goeppert-Str. 5, 23562 Lübeck, Germany
[b]Institut für Biomedizinische Optik, Peter-Monnig-Weg 4, 23562 Lübeck, Germany
[c]Medizinisches Laserzentrum Lübeck, Peter-Monnig-Weg 4, 23562 Lübeck, Germany

ABSTRACT

We demonstrate a full-field swept-source OCT using an off-axis geometry of the reference illumination. By using holographic refocusing techniques, a uniform lateral resolution is achieved over the measurement depth of approximately 80 Rayleigh lengths. Compared to a standard on-axis setup, artifacts and autocorrelation signals are suppressed and the measurement depth is doubled by resolving the complex conjugate ambiguity. Holographic refocusing was done efficiently by Fourier-domain resampling as demonstrated before in inverse scattering and holoscopy. It allowed to reconstruct a complete volume with about 10 μm resolution over the complete measurement depth of more than 10 mm. Off-axis full-field swept-source OCT enables high measurement depths, spanning many Rayleigh lengths with reduced artifacts.

Keywords: Optical coherence tomography, Fourier-domain, full-field, full-range, digital holography

1. INTRODUCTION

With the invention of Fourier-domain optical coherence tomography (OCT) the measurement speed was considerably increased compared to time-domain OCT (TD-OCT) as all depths are acquired in parallel. Despite of its obvious capabilities, scanning FD-OCT still faces many challenges: In FD-OCT the focus and the confocal gating remain fixed, effectively limiting the optimal imaging depth to a few Rayleigh lengths. Increased imaging speed of FD-OCT is purchased by autocorrelation artifacts (coherence noise) decreasing imaging quality, especially for highly scattering and reflecting specimen (Fig. 1a). Additionally, in OCT lateral scanning mechanisms limit the effective acquisition speed.

Full-field swept-source OCT (FF-SS-OCT) allows parallelizing acquisition without requiring a lateral scanning mechanism.[1,2] It extends the limitations on the allowed light exposition on the sample (maximum permissible exposure, MPE). Consequently, FF-SS-OCT allows a significant increase in imaging speed. On the downside, it is also more sensitive to coherent and incoherent background noise, as more stray light and parasitic reflexes reach the camera. Incoherent light thereby introduces an increased noise floor, coherent background causes image artifacts, such as horizontal lines (Fig. 1b).

Numerical refocusing techniques, as used in digital holography,[4–9] inverse scattering,[10–12] and holoscopy[13–15] increase the effective focus depth to more than a few Rayleigh lengths with constant diffraction limited resolution and uniform sensitivity. FF-SS-OCT thus allows fast tomographic imaging over many Rayleigh lengths without requiring axial scanning. In a standard Michelson-type setup (see Fig. 2), reference and sample light illuminate the camera under the same angle (on-axis), whereas in an off-axis setup the reference illuminates the camera under a different angle, as demonstrated for a Mach-Zehnder type setup in Fig. 7. Here, we show that by using such an off-axis setup, similar to Hilbert phase microscopy[16] and digital holographic microscopy,[4,5] autocorrelation artifacts can be suppressed. Artifacts that are introduced by the setup, such as lines from reflections of optical components, as for example of the protective glass of the image sensor, can be removed. In addition, the measurement depth can be doubled as the off-axis reference beam resolves the complex conjugate ambiguity similar to full-range OCT.[17,18]

*dhillmann@thorlabs.com; phone +49 451 2903256

Optical Coherence Tomography and Coherence Domain Optical Methods in Biomedicine XVII,
edited by James G. Fujimoto, Joseph A. Izatt, Valery V. Tuchin, Proc. of SPIE Vol. 8571, 857104
 · doi: 10.1117/12.2006436

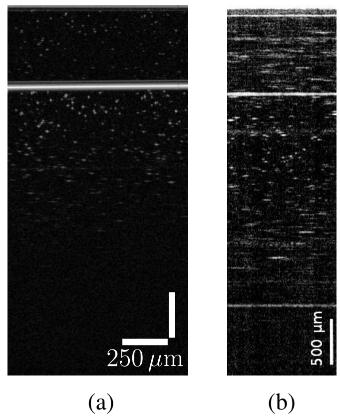

Figure 1: a) B-scan of a phantom of 300nm–800nm sized iron oxide particles, embedded in polyurethane resin.[3] Limitations of scanning FD-OCT can be seen: Scattering nanoparticles are only clearly visible close to the focus of the imaging optics. Outside the lateral resolution and sensitivity degrade. Autocorrelation artifacts appear as images of point scatterers above its upper surface (horizontal line). b) Full-field SS-OCT B-scan of the same sample. Artifacts caused by coherent background light show up as horizontal lines in the image. Although sensitivity does no longer degrade outside of the focus region, diffraction limited lateral resolution is still restricted to the Rayleigh range.

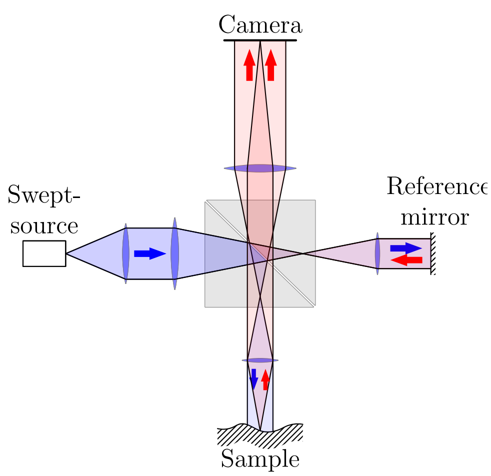

Figure 2: Setup of a standard full-field swept-source OCT system. In an open Michelson-type setup, the sample is illuminated by a collimated beam, and the backscattered light is imaged onto an area camera, where it interferes with collimated reference light.

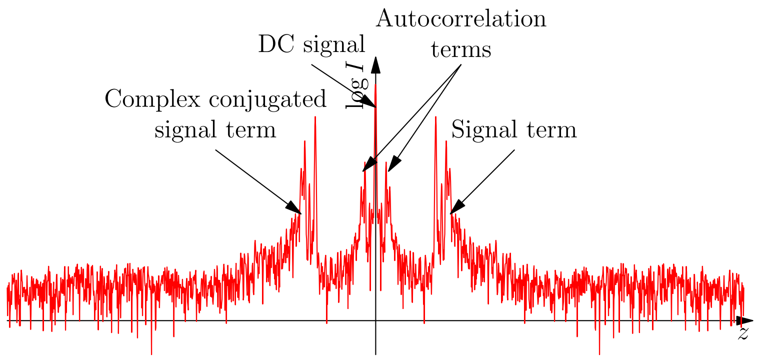

Figure 3: A typical A-scan of an FD-OCT system. The different terms of the interference signals can be distinguished, but they influence imaging quality and cause artifacts. The complex conjugate signal term can overlay the signal term and distort the image information.

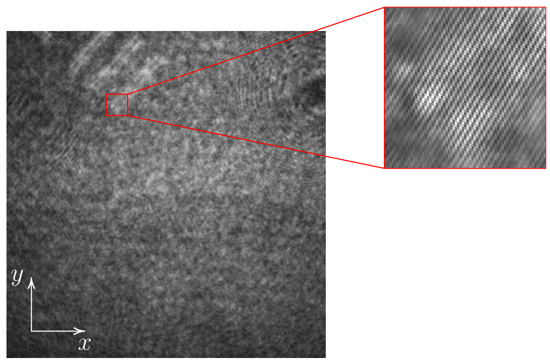

Figure 4: Image, as acquired by the off-axis full-field setup (left). The carrier frequency due to the off-axis illumination becomes visible in the zoomed image (right).

2. PRINCIPLE

OCT works by acquiring the interference signal I between waves originating from the sample O and a reference wave R. In FD-OCT, this signal is acquired spectrally resolved, and after a Fourier transform the various signal terms can be distinguished (see also Fig. 3). The interference term is given by

$$I \propto |R+O|^2 = |R|^2 + |O|^2 + R^*O + RO^*,$$

where $|R|^2 + |O|^2$ denotes DC and autocorrelation terms, R^*O is the signal term and RO^* its complex conjugate. In general the DC and autocorrelation term do not carry the desired A-scan information. The signal term and the conjugate signal term can only be distinguished, if sample arm path-lengths are always ensured to be longer than the reference path length or vice versa. If this is not in the case, the signals above and below the reference plane will overlap with each other, and imaged structures can not be clearly identified.

With the proposed setup, there is a small angle between reference and sample light reaching the camera. As the light interferes, this causes interference fringes and effectively results in a carrier frequency on the sample light field. The carrier frequency, which is demonstrated in Fig. 4, causes the signal term R^*O, and its complex conjugate to be shifted away from the DC-component into opposite directions after a two-dimensional Fourier transform (Fig. 5). Combining this lateral discrimination of the signal terms with the axial discrimination of the OCT signal terms, as shown in Fig. 6, the terms are separated. The complex conjugate ambiguity is resolved by filtering one of the two signal terms, effectively increasing the measurement depth. As DC and autocorrelation signals are still centered and not shifted, they do not overlay with the signal terms and are also removed, which reduces coherent imaging artifacts.

Without restrictions to the measuring depth by confocal gating, and by resolving the complex conjugate ambiguity and therefore halving the influence of the limited instantaneous coherence length of the laser, the achievable imaging depth is largely increased. Finally, by using holographic refocusing,[12,15,19] the limitations on the optimal lateral resolution to the Rayleigh length is effectively removed.

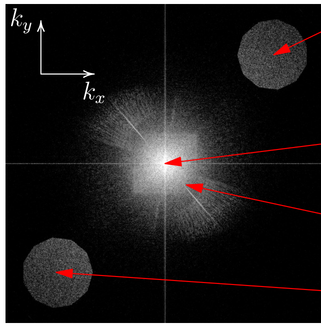

Figure 5: Fourier transforming the acquired images, the different signal terms can be distinguished. The DC and autocorrelation terms are centered in the image, the signal term and its complex conjugate are visible as circles in the upper right and lower left corner, respectively. The circular shape of the signal terms is caused by the aperture placed in the Fourier conjugated plane of the image/object.

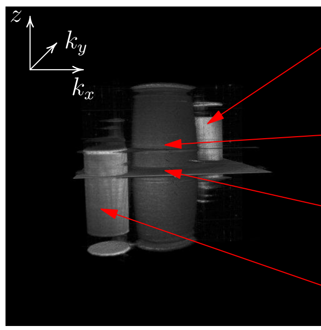

Figure 6: Combining two-dimensional FFT of acquired images as shown in Fig. 5 with the axial discrimination in an OCT A-scan (Fig. 3) shows that signal term, its complex conjugate, and the autocorrelation term can clearly be distinguished. Suitable filtering can select one of the two signal terms and suppress other signals.

3. SETUP

The setup we used for off-axis full-field swept-source OCT was a Mach-Zehnder type setup as shown in Fig. 7. As tunable laser we used a Broadsweeper BS-840-1 (Superlum, Ireland) with a tuning range from 867 nm to 816 nm and 3 mW output power. Its light was split by a fiber coupler in reference and sample arm. The reference light was collimated to a beam with about 16 mm diameter and illuminated the camera under a slight angle of approximately 3°. The sample was illuminated by collimated light and the backscattered light was imaged onto the camera using a two lens telescope, with a circular aperture in the Fourier plane of the imaging lens. The circular aperture effectively limited the NA of the setup and ensured correct sampling of interference fringes on the camera. A Basler ACE camera (acA2040-180km, Basler, Germany) with 2048×2048 pixels of size $5.5\,\mu\text{m} \times 5.5\,\mu\text{m}$ each was used. Different areas of interest (AOI) were selected to adjust acquisition speed and field of view. The sweep of the laser and the acquisition of the camera were hardware synchronized, by triggering the laser with the camera. Images were acquired with a numerical apertures (NA) of up to 0.08.

4. RESULTS

The effect of the lateral filtering is shown in Fig. 8. A scotch tape was acquired at approximately NA 0.04 by the off-axis FF-SS-OCT setup, and reconstructed without applying the lateral filtering for removing the autocorrelation and conjugated term (Fig. 8a). The images are thus comparable to images, acquired with a standard Michelson-type setup. Fig. 8b shows the same dataset with the lateral filter applied. Here, horizontal lines and coherence noise are significantly reduced. Finally, Fig. 8c shows the scotch tape with the complex conjugate ambiguity resolved, measurement depth could be increased, although the central DC line is still visible. The proposed technique can also be used to image more complex structures, as shown in Fig. 9. Here, a 3D-rendering of an off-axis FF-SS-OCT volume of a bug is shown.

Fig. 10a shows the increased measurement depth for a scattering phantom, containing 300 nm to 800 nm sized iron oxide nanoparticles embedded in polyurethane resin, acquired at NA 0.08. Almost in the entire depth of the sample (about

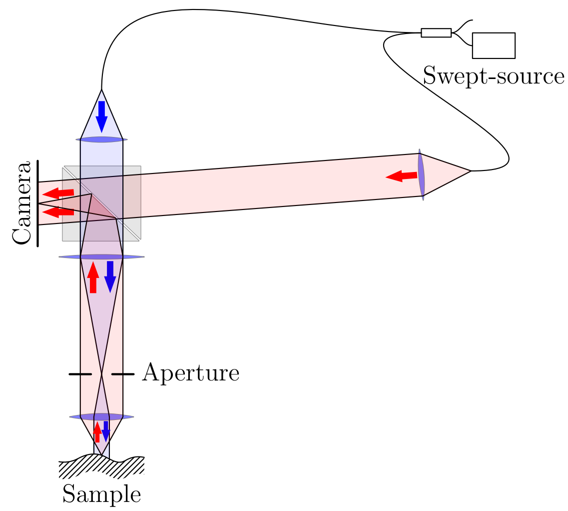

Figure 7: Setup for an off-axis full-field swept-source system. The collimated reference light illuminates the camera under a slight angle.

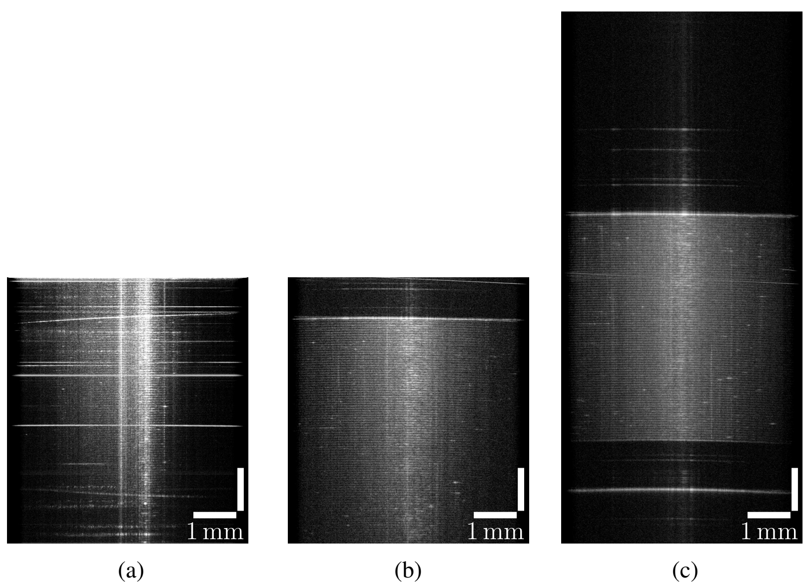

Figure 8: Images of scotch tape, acquired by off-axis FF-SS-OCT. a) B-scan as obtained when no filtering is applied. b) B-scan with lateral filtering applied. c) B-scan showing positive and negative path length differences of the sample light. The complex conjugate ambiguity of FD-OCT is resolved by filtering the signal term.

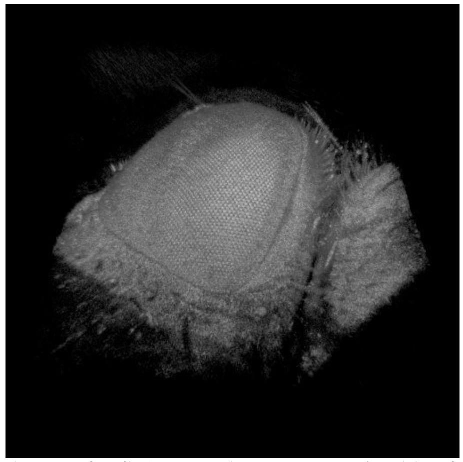

Figure 9: Rendering of a volume of a fly's eye, that was acquired by full-field swept-source OCT.

10 mm) the point scatterers are visible, which corresponds to about 15 mm imaging in air. The DC part of signal is not suppressed well and can clearly be seen in the middle of the imaging depth. Signal of the point scatterers is highest in the central part of the image, and degrades outwards due to the limited coherence length of the laser (signal roll-off). In the entire B-scan, only in a small layer the point scatterers are shown with a good resolution due to the limited depth of focus. Fig. 10b shows the effect of holographic refocusing, by resampling in Fourier-space to obtain diffraction limited resolution over the entire measurement depth. Using this technique, lateral and axial resolution of about 10 μm in the medium ($n \approx 1.5$), could be extended to the entire image which covered almost 10 mm (about 15 mm in air) imaging depth. With the corresponding Rayleigh length of $2z_R \approx 125\,\mu$m imaging was performed over 80 Rayleigh lengths.

Fig. 11a demonstrates off-axis FF-SS-OCT at NA 0.04 for imaging of the anterior segment of a porcine eye. The sweep range of the laser was reduced to 30 nm. Although cornea and front surface of the lens are clearly visible, contrast and dynamic range of the image is limited. As illustrated in Fig. 11b the collimated light on the eye illuminates only a single spot on the retina. Light scattered from here reaches also the camera, due to the lack of a confocal gating, and causes incoherent noise. By further extending the measurement depth, reducing the laser sweep range to 25 nm, and additionally squeezing the eye in axial direction, the entire eye including retina was imaged (Fig. 12). Now the light, scattered by the retina was no longer incoherent, and the dynamic range of the images increased significantly. Front and back surface of the lens were clearly seen. The loss in signal in the front surface is caused by the roll-off due to the limited coherence length of the laser. The resulting image corresponds to an imaging depth of more than 30 mm in air.

5. CONCLUSION

In conclusion, we demonstrated an off-axis setup for full-field swept-source OCT, which abolishes many shortcomings of scanning and full-field SS-OCT. It extends the focal range, sensitivity and lateral resolution are maintained over an extended depth spanning approximately 80 Rayleigh lengths. The off-axis setup allows for removing autocorrelation terms and artifacts. Additionally, it resolves the complex conjugate ambiguity and thus allows full-range imaging, without requiring any moving parts in the setup.

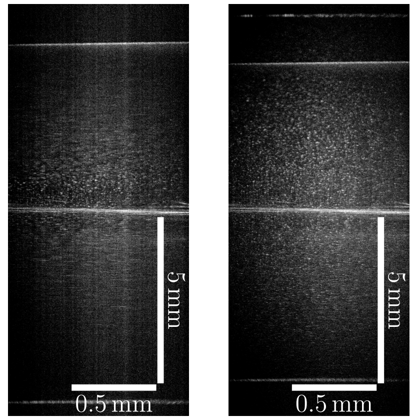

(a) (b)

Figure 10: Images of the phantom of point scattering nanoparticles as shown in Fig. 1a and Fig. 1b over a large measurement depth of almost 10 mm. The DC signal in the middle of the images is clearly visible. a) Without applying holographic refocusing techniques, only a small layer of point scatterers can be imaged with good resolution. b) When using holographic refocusing, the entire measurement depth can be imaged with almost the same resolution.

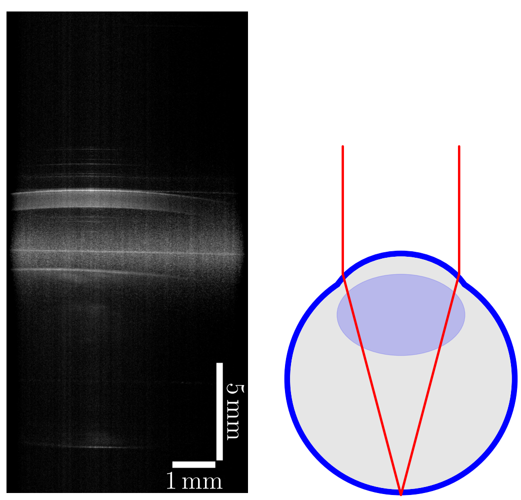

(a) (b)

Figure 11: a) B-scans of the anterior segment of a porcine eye, acquired by off-axis FF-SS-OCT. Cornea, front and back surface of the lens are visible, although dynamic range is reduced. b) Collimated light illuminated the eye and formed a single spot on the retina. The light backscattered by the retina leaves the eye again as a parallel beam, and reaches the area camera.

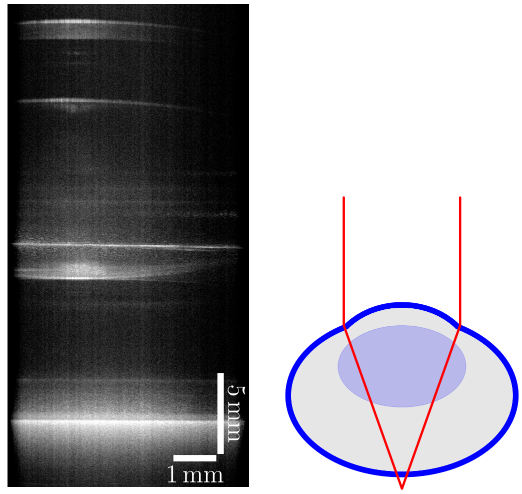

(a) (b)

Figure 12: a) B-scans of the eye of a porcine eye, acquired by off-axis FF-SS-OCT. Compared to Fig. 11a, the entire eye is visible and thus backscattered light from the retina reaching the camera is coherent and forms an image at the correct depth. Consequently imaging quality is improved; cornea, front and back surface of the lens are clearly visible. b) To image the complete eye it had to be is squeezed.

REFERENCES

[1] Považay, B., Unterhuber, A., Hermann, B., Sattmann, H., Arthaber, H., and Drexler, W., "Full-field time-encoded frequency-domain optical coherence tomography," *Opt. Express* **14**(17), 7661–7669 (2006).

[2] Bonin, T., Franke, G., Hagen-Eggert, M., Koch, P., and Hüttmann, G., "In vivo Fourier-domain full-field OCT of the human retina with 1.5 million A-lines/s," *Opt. Lett.* **35**(20), 3432–3434 (2010).

[3] Woolliams, P. D., Ferguson, R. A., Hart, C., Grimwood, A., and Tomlins, P. H., "Spatially deconvolved optical coherence tomography," *Appl. Opt.* **49**, 2014–2021 (Apr 10 2010).

[4] Schnars, U. and Jueptner, W., [*Digital holography: digital hologram recording, numerical reconstruction, and related techniques*], Springer (2005).

[5] Kim, M., [*Digital Holographic Microscopy: Principles, Techniques, and Applications*], Springer Series in Optical Sciences, Springer (2011).

[6] Zvyagin, A. V., "Fourier-domain optical coherence tomography: optimization of signal-to-noise ratio in full space," *Opt. Commun.* **242**(1-3), 97–108 (2004).

[7] Kim, M. K., "Wavelength-scanning digital interference holography for optical section imaging," *Opt. Lett.* **24**, 1693–1695 (Dec 1999).

[8] Potcoava, M. C. and Kim, M. K., "Optical tomography for biomedical applications by digital interference holography," *Meas. Sci. Technol.* **19**(7), 074010 (2008).

[9] Moiseev, A. A., Gelikonov, G. V., Shilyagin, P. A., Terpelov, D. A., and Gelikonov, V. M., "Digital refocusing in optical coherence tomography," *Proc. SPIE* **8213**(1), 82132C (2012).

[10] Ralston, T. S., Marks, D. L., Scott Carney, P., and Boppart, S. A., "Interferometric synthetic aperture microscopy," *Nat. Phys.* **3**(2), 129–134 (2007). 10.1038/nphys514.

[11] Ralston, T. S., Marks, D. L., Carney, P. S., and Boppart, S. A., "Real-time interferometric synthetic aperture microscopy," *Opt. Express* **16**, 2555–2569 (Feb 18 2008).

[12] Marks, D. L., Ralston, T. S., Boppart, S. A., and Carney, P. S., "Inverse scattering for frequency-scanned full-field optical coherence tomography," *J. Opt. Soc. Am. A* **24**(4), 1034–1041 (2007).

[13] Hillmann, D., Lührs, C., Bonin, T., Koch, P., and Hüttmann, G., "Holoscopy—holographic optical coherence tomography," *Opt. Lett.* **36**, 2390–2392 (Jul 2011).

[14] Franke, G. L., Hillmann, D., Claußen, T., Lührs, C., Koch, P., and Hüttmann, G., "High resolution holoscopy," *Proc. SPIE* **8213**(1), 821324 (2012).

[15] Hillmann, D., Franke, G., Lührs, C., Koch, P., and Hüttmann, G., "Efficient holoscopy image reconstruction," *Opt. Express* **20**, 21247–21263 (Sep 2012).

[16] Ikeda, T., Popescu, G., Dasari, R. R., and Feld, M. S., "Hilbert phase microscopy for investigating fast dynamics in transparent systems," *Opt. Lett.* **30**, 1165–1167 (May 2005).

[17] Yasuno, Y., Makita, S., Endo, T., Aoki, G., Itoh, M., and Yatagai, T., "Simultaneous B-M-mode scanning method for real-time full-range Fourier domain optical coherence tomography," *Appl. Opt.* **45**, 1861–1865 (Mar 2006).

[18] Jungwirth, J., Baumann, B., Pircher, M., Götzinger, E., and Hitzenberger, C. K., "Extended in vivo anterior eye-segment imaging with full-range complex spectral domain optical coherence tomography," *J. Biomed. Opt.* **14**(5), 050501–050503 (2009).

[19] Davis, B. J., Marks, D. L., Ralston, T. S., Carney, P. S., and Boppart, S. A., "Interferometric synthetic aperture microscopy: Computed imaging for scanned coherent microscopy," *Sensors* **8**(6), 3903–3931 (2008).